INTERFACIAL CONFINEMENT IN SEMI-CRYSTALLINE SHAPE MEMORY POLYMER TOWARDS SEQUENTIALLY DYNAMIC RELAXATIONS*

Jingyun Liu[1], Ziyu Xing[1], Xiaodong Wang[1], Haibao Lu[1,†] and Yong Qing Fu[2,‡]

1National Key Laboratory of Science and Technology on Advanced Composites in Special Environments, Harbin Institute of Technology, Harbin 150080, China

2Faculty of Engineering and Environment, Northumbria University, Newcastle upon Tyne, NE1 8ST, UK§

†*luhb@hit.edu.cn*

‡*richard.fu@northumbria.ac.uk*

Received Day Month Year
Revised Day Month Year

Sequential glass and melting transitions in semi-crystalline shape memory polymers (SMPs) provide great opportunities to design and generate multiple shape-memory effects (SMEs) for practical applications. However, the complexly dynamic confinements of coexisting amorphous and crystalline phases within the semi-crystalline SMPs are yet fully understood. In this study, an interfacial confinement model is formulated to describe dynamic relaxation and shape memory behavior in the semi-crystalline SMPs undergoing sequential phase/state transitions. A confinement entropy model is firstly established to describe the glass transition behavior of amorphous phase within the SMPs based on the free volume theory, where the free volume is critically confined by the crystalline phase. An extended Avrami model is then formulated using the frozen volume theory to characterize the melting and crystallization transitions of the crystalline phase in the SMPs, whose interfacial confinement with the amorphous phase has been identified as the driving force for the supercooled regime. Furthermore, an extended Maxwell model is formulated to describe the effect of dynamic confinement of two phases on the multiple SMEs and shape recovery behaviors in the semi-crystalline SMPs. Finally, effectiveness of the newly proposed model is verified using the experimental data reported in the literature. This study aims to provide a new methodology for the dynamic confinements and cooperative principles in the semi-crystalline SMP towards multiple SMEs.

Keywords: shape memory polymer; semi-crystalline; dynamic confinement.

* For the title, try not to use more than 3 lines. Typeset the title in 10 pt Times Roman, uppercase and boldface.
† State completely without abbreviations, the affiliation and mailing address, including country. Typeset in 8 pt Times Italic.
‡ State completely without abbreviations, the affiliation and mailing address, including country. Typeset in 8 pt Times Italic.
§ Typeset names in 8 pt Times Roman, uppercase. Use the footnote to indicate the present or permanent address of the author.

Nomenclature

p_j	The probability of an amorphous phase to relax
p_e and p_v	The probability of the amorphous phase to obtain sufficient activation energy to overcome the energy barrier and enough free volume available to jump, respectively
t	Time
T	Temperature
T_0	The initial temperature
T_m	The melting temperature
	The melting temperature of infinite crystal
T_c	The crystallizing temperature
$\dot{T}$	Heating rate
F_a	Activation energy
R	The molar gas constant
V_f	The free volume
V_0	The volume occupied by the amorphous phase
V_a	The volume occupied by the amorphous phase and the free volume
V_c	The volume for crystalline phase
α_g and α_r	The thermal expansion coefficients of amorphous phase in glassy and rubbery states, respectively
s^*	The maximum conformational entropy of 1 mol amorphous phase
S_c	The conformational entropy of 1 mol amorphous phase
$\Delta\mu$	The average activation energy of 1 mol amorphous phase
S_d	Disorientation entropy
S_{ce}	Confinement entropy
S_i	Interfacial entropy
S_{mix}	Mixing entropy
φ_a and φ_c	The volume fractions of amorphous and crystalline phases, respectively
r_a and r_c	The molar volume ratios of amorphous and crystalline phases, respectively
R_c and r_0	The radii of the crystalline phase and semi-crystalline chain, respectively
γ_i	The proportionality constant of the interfacial interaction between amorphous and crystalline phases
γ_e	The free energy of interfacial melt-crystal phase
z	The lattice coordination number
ϕ_a	The phase evolution function of amorphous phase
	The volume evolution function of crystalline phase
$\varepsilon_{s,a}$ and $\varepsilon_{pre,a}$	The stored strain and pre-stored strain of amorphous phase, respectively
$\varepsilon_{s,c}$ and $\varepsilon_{pre,c}$	The stored strain and pre-stored strain of crystalline phase, respectively

ε_s and ε_{s0}	The stored strain and pre-stored strain of semi-crystalline, respectively
K_{max}	The kinetic parameter of the melting transition
l_c	The dimension of the single crystal
ΔH_f	The fusion heat
$E_a(T)$ and $E_c(T)$	The storage moduli of the amorphous and crystalline phases in a semi-crystalline SMP, respectively
E_{a0} and E_{c0}	The initial storage modulus of the amorphous and crystalline phases in a semi-crystalline SMP, respectively
n_a and n_c	The numbers of the glass and melting transitions in the semi-crystalline SMP, respectively
i and j	i represents the ith glass transition of the amorphous phase, j represents the jth melting transition of the crystalline phase
$t_{a,i}$ and $t_{c,j}$	The starting times of the ith glass transition and jth melting transition, respectively
$\tau_{0,a,i}$ and $\tau_{0,c,j}$	The relaxation times of the ith glass transition of amorphous transition and jth melting transition, respectively
A_0, m, γ and D	The material constants

1. Introduction

Shape memory polymer (SMP) is one of the most popular stimulus-responsive materials which have capabilities of regaining their permanent shapes after deformation only when exposed to external stimuli [Fang *et al.*, 2015], such as heat, solvent, light, electric or magnetic fields [Cho *et al.*, 2005; Huang *et al.*, 2020; Hu *et al.*, 2021; Ji *et al*, 2017; Lu *et al.*, 2011; Yang *et al.*, 2004]. The shape memory effect (SME) in most SMPs can be triggered by heating them above their either glass or melting transition temperatures [Meng *et al.*, 2013]. The capability of SMPs to recover to original shapes from their pre-deformed shapes, in responses to the proper stimuli, gives rise to a great number of practical applications in actuators [Wang *et al.*, 2012; Zhang *et al.*, 2019], textile [Vili *et al.*, 2007], deployable structures [Santo *et al.*, 2012] and biomedical devices [Ortega *et al.*, 2013].

Compared with the conventional SMPs which are based on only glass transition temperature (T_g) or melting transition temperature (T_m) with a narrow range (typically≤30 K) [Xie, 2010], semi-crystalline SMPs could have two or more distinct thermal transitions over a large temperature range (typically ≥ 80 K) because of their coexisting amorphous and crystalline phases [Zhou *et al.*, 2018]. Their multiple glass and melting transitions expand the width of shape memory transition temperature region and enable their multiple SMEs [Bellin *et al.*, 2006; Qin *et al.*, 2009]. In terms of thermodynamics, the SME of the amorphous phase in the semi-crystalline SMP is originated from its relaxation behavior [Fang *et al.*, 2018; Zheng *et al.*, 2021] which is essentially determined by the free volume of SMP [Hamonic *et al.*, 2014; Jäckle, 1986; Scalet *et al.*, 2018]. On the other hand, dynamic melting transition of the crystalline phase is significantly influenced by the interfacial confinements between the amorphous and crystalline phases [Hui *et al.*, 2020;

Scalet *et al.*, 2018]. Therefore, both the glass transition and melting transition are determined by dynamically interfacial confinements of these two phases [Fang *et al.*, 2018], which are the key factors taken into consideration for modelling the SME in the semi-crystalline SMP [Hamonic *et al.*, 2014; Jäckle, 1986]. However, there are few studies carried out on this topic, and its working principle has not been well explored.

In this paper, we formulate a dynamic confinement model to describe the multiple SMEs and thermodynamic characteristics of the semi-crystalline SMPs. Confinement entropy [Gibbs *et al.*, 1965; Lee *et al.*, 2010] and free volume theory [Macedo *et al.*, 1965] are initially employed to characterize the glass transition of amorphous phase in the semi-crystalline SMPs, whose dynamic glass transition is confined by the crystalline phase in terms of free volume. Then the modified Avrami theory is proposed to explore the working principles of melting and crystallization transitions of the crystalline phase in the SMPs, whose dynamic melting transition is also confined by the amorphous phase at their interfaces [Avrami, 1939]. Furthermore, the multiple SMEs and dynamic behaviors are investigated using the newly proposed model based on the Maxwell principles [Dickie, 1973; Treloar, 2005]. Finally, the analytical results obtained using our new model are compared with the experimental data reported in Ref. [Hui *et al.*, 2020; Luo *et al.*, 2010; Scalet *et al.*, 2018; Zhou *et al.*, 2018] for verifications.

2. Theoretical framework

2.1. *Dynamic confinement of glass transition*

Thermomechanical behavior of the semi-crystalline polymer is critically determined by the glass and melting transitions of coexisting amorphous and crystalline phases. Therefore, shape memory behavior of the semi-crystalline SMP is essentially dependent on the thermodynamics of both glass and melting transitions, which are illustrated in Fig. 1. Moreover, the shape recovery strain and programming strain during the transitions are also shown in Fig.1.When the ambient temperature is higher than the T_g of semi-crystalline SMP, its free volume is increased which can trigger the shape memory behavior of the amorphous phase. With a further increase in the temperature above the T_m of the crystalline phase, its shape memory is triggered. Meanwhile, by decreasing the temperature below the T_g and T_m in a sequence, the semi-crystalline SMP can be gradually programmed as its temporary shapes. Therefore, a dual-SME has been achieved based on the coexisting amorphous and crystalline phases through their sequential glass and melting transitions in the semi-crystalline SMP.

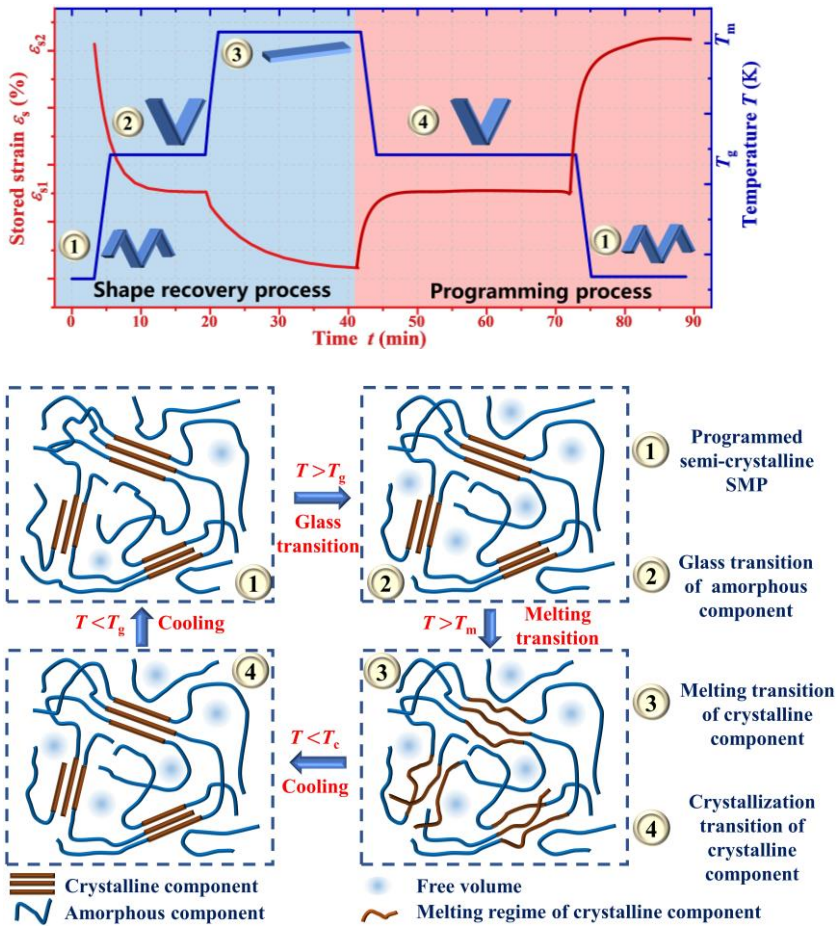

Fig. 1. Schematic illustrations of glass and melting transitions of coexisting amorphous and crystalline phases in semi-crystalline SMP undergoing dual-SME.

For the amorphous phase, it needs both activation energy and free volume of the SMP for its glass transition. The probability (p_j) of an amorphous phase to relax around the T_g can be written as [Macedo *et al.*, 1965],

$$p_j = p_e \cdot p_v \tag{1}$$

where p_e is the probability of the amorphous phase to obtain sufficient activation energy to overcome the energy barrier, and p_v is the probability of the amorphous phase to obtain enough free volume available to jump [Macedo *et al.*, 1965].

p_e can be expressed by Eyring equation as follows [Adams *et al.*, 1978],

$$p_e = A_0 T^m \exp\left(-\frac{F_a}{RT}\right) \tag{2}$$

where A_0 is the material constant, T (K) is the temperature, m is a given coefficient, F_a is

the activation energy and R=8.314J/(mol·K) is the molar gas constant.

p_v, the probability of relaxation determined by the free volume (V_f) [Cohen *et al.*, 1959], can be obtained based on the Arrhenius equation [Schweizer *et al.*, 2004] and Adam-Gibbs' model [Macedo *et al.*, 1965],

$$p_v = \exp\left(\frac{-\gamma V_0}{V_f}\right) = \exp\left(-\frac{s^*}{S_c}\cdot\frac{\Delta\mu}{RT}\right) \tag{3}$$

where γ is a given numerical factor ($0.5 \le \gamma \le 1$) [Cohen *et al.*, 1959], V_0 is the volume occupied by the amorphous phase, s^* is the maximum conformational entropy of 1 mol amorphous phase, in which the conformers relax independently [Schweizer *et al.*, 2004], S_c is the conformational entropy of 1 mol amorphous phase, in which all the conformers relax cooperatively [Schweizer *et al.*, 2004], and $\Delta\mu$ is the average activation energy of 1 mol amorphous phase [Schweizer *et al.*, 2004].

According to the Doolittle equation [Doolittle *et al.*, 1951; Gibbs *et al.*, 1965], V_f is originated from the thermal expansion of semi-crystalline SMP under the atmospheric pressure,

$$\begin{aligned} V_f &= V_a - V_0 = V_0\left\{\exp\left[\int_0^T \alpha(T)\,dT\right]-1\right\} \\ &= V_0\left[\exp\left(\int_0^{T_0}\alpha\,dT + \int_{T_0}^{T_g}\alpha_g\,dT + \int_{T_g}^{T}\alpha_r\,dT\right)-1\right] \approx V_0\left[\exp\left(\alpha_r T - \alpha_g T_0\right)-1\right] \end{aligned} \tag{4}$$

where V_a is the volume occupied by the amorphous phase and the free volume at the temperature of T, T_0 is the initial temperature, α_g and α_r are the volume thermal expansion coefficients of amorphous phase in glassy and rubbery states, respectively [Treloar, 2005].

In combination of equations (3) and (4), the conformational entropy (S_c) can be written as,

$$S_c = \frac{s^*\Delta\mu}{\gamma RT}\cdot\left[\exp\left(\alpha_r T - \alpha_g T_0\right)-1\right] \tag{5}$$

Different from the amorphous one, the total volume of semi-crystalline polymer is composed of three parts: the free volume (V_f), the volume occupied by amorphous phase (V_0) and the volume for crystalline phase (V_c). Here, the p_v of semi-crystalline polymer can therefore be rewritten as,

$$p_v = \exp\left[\frac{-\gamma\left(V_0+V_c\right)}{V_f}\right] = \exp\left(-\frac{s^*}{S_c}\cdot\frac{\Delta\mu}{RT}\right) \tag{6}$$

where S_c is the conformational entropy of 1 mol semi-crystalline polymer.

In semi-crystalline polymer, four types of conformational entropies should be considered [Lee *et al.*, 2010]: disorientation entropy (S_d), confinement entropy (S_{ce}), interfacial entropy (S_i) and mixing entropy (S_{mix}). Meanwhile, confinement entropy (S_{ce}) and interfacial entropy (S_i) both are used to restrict the relaxation of amorphous phase, while the mixing entropy (S_{mix}) is able to promote the relaxation [Lee *et al.*, 2010; Wang *et al.*, 2021],

$$\begin{cases} S_{ce} = -R\dfrac{\varphi_c}{r_c}\left[\ln\varphi_c + \tanh\left(\dfrac{R_c}{r_0}-1\right)\dfrac{4\varphi_c-3\varphi_c^2}{\varphi_a^2}\right] \\ S_i = R\gamma_i \ln\left(\dfrac{z-1}{e}\right)\left(\dfrac{\varphi_a}{r_a}\ln\varphi_a + \dfrac{\varphi_c}{r_c}\ln\varphi_c\right) \\ S_{mix} = -R\left(\dfrac{\varphi_a}{r_a}\ln\varphi_a + \dfrac{\varphi_c}{r_c}\ln\varphi_c\right) \end{cases} \tag{7}$$

where φ_a and φ_c are the volume fractions of amorphous and crystalline phases, respectively. r_a and r_c are the molar volume ratios of amorphous and crystalline phases, respectively [Wang *et al.*, 2021]. R_c and r_0 are the radii of the crystalline phase and semi-crystalline chain, respectively [Ginzburg, 2005]. γ_i is the proportionality constant of the interfacial interaction between amorphous and crystalline phases [Ginzburg, 2005] and z is the lattice coordination number.

In combination of equations (5) and (7), the conformational entropy (S_c) can be written as,

$$\begin{aligned} S_c &= \varphi_a S_d + S_{ce} + S_i + S_{mix} \\ &= \varphi_a \cdot \frac{s^*\Delta\mu}{\gamma RT}\cdot\left[\exp\left(\alpha_r T - \alpha_g T_0\right)-1\right] - R\frac{\varphi_c}{r_c}\left[\ln\varphi_c + \tanh\left(\frac{R_c}{r_0}-1\right)\frac{4\varphi_c-3\varphi_c^2}{\varphi_a^2}\right] \\ &\quad + R\left[\gamma_i \ln\left(\frac{z-1}{e}\right)-1\right]\left(\frac{\varphi_a}{r_a}\ln\varphi_a + \frac{\varphi_c}{r_c}\ln\varphi_c\right) \end{aligned} \tag{8}$$

By substituting equation (8) into (6), the p_v of amorphous phase can be obtained as,

$$\begin{aligned} p_v &= \exp\left[\frac{-\gamma\left(V_0+V_c\right)}{V_f}\right] = \exp\left(-\frac{s^*}{S_c}\cdot\frac{\Delta\mu}{RT}\right) \\ &= \exp\left\{\begin{array}{l} \dfrac{R^2T}{s^*\Delta\mu}\cdot\dfrac{\varphi_c}{r_c}\left[\ln\varphi_c + \tanh\left(\dfrac{R_c}{r_0}-1\right)\dfrac{4\varphi_c-3\varphi_c^2}{\varphi_a^2}\right] - \dfrac{\varphi_a}{\gamma}\cdot\left[\exp\left(\alpha_r T-\alpha_g T_0\right)-1\right] \\ + \dfrac{R^2T}{s^*\Delta\mu}\cdot\left[1-\gamma_i\ln\left(\dfrac{z-1}{e}\right)\right]\left(\dfrac{\varphi_a}{r_a}\ln\varphi_a + \dfrac{\varphi_c}{r_c}\ln\varphi_c\right) \end{array}\right\}^{-1} \end{aligned} \tag{9}$$

In combination of equations (1), (2) and (9), the probability of amorphous phase to relax, p_j, can be expressed as follows,

$$\begin{aligned} p_j &= p_e \cdot p_v \\ &= A_0 T^m \exp\left(-\frac{F_a}{RT}\right) \\ &\cdot \exp\left\{\begin{array}{l} \dfrac{R^2T}{s^*\Delta\mu}\cdot\dfrac{\varphi_c}{r_c}\left[\ln\varphi_c + \tanh\left(\dfrac{R_c}{r_0}-1\right)\dfrac{4\varphi_c-3\varphi_c^2}{\varphi_a^2}\right] - \dfrac{\varphi_a}{\gamma}\cdot\left[\exp\left(\alpha_r T-\alpha_g T_0\right)-1\right] \\ + \dfrac{R^2T}{s^*\Delta\mu}\cdot\left[1-\gamma_i\ln\left(\dfrac{z-1}{e}\right)\right]\left(\dfrac{\varphi_a}{r_a}\ln\varphi_a + \dfrac{\varphi_c}{r_c}\ln\varphi_c\right) \end{array}\right\}^{-1} \end{aligned} \tag{10}$$

According to the frozen volume theory [Liu *et al.*, 2006], the phase evolution function of amorphous phase (ϕ_a) is determined by the stored strain ($\varepsilon_{s,a}$) and pre-stored strain ($\varepsilon_{pre,a}$) with the expression as follows,

$$\phi_a = \frac{\varepsilon_{s,a}}{\varepsilon_{pre,a}} = 1 - p_j \tag{11}$$

By substituting equation (10) into (11), the volume evolution function of amorphous phase (ϕ_a) can be written as,

$$\begin{aligned}\phi_a &= \frac{\varepsilon_{s,a}}{\varepsilon_{pre,a}} = 1 - p_j \\ &= 1 - A_0 T^m \exp\left(-\frac{F_a}{RT}\right) \\ &\cdot \exp\left\{\frac{R^2T}{s^*\Delta\mu}\cdot\frac{\varphi_c}{r_c}\left[\ln\varphi_c + \tanh\left(\frac{R_c}{r_0}-1\right)\frac{4\varphi_c - 3\varphi_c^2}{\varphi_a^2}\right] - \frac{\varphi_a}{\gamma}\cdot\left[\exp\left(\alpha_r T - \alpha_g T_0\right) - 1\right]\right. \\ &\left. + \frac{R^2T}{s^*\Delta\mu}\cdot\left[1 - \gamma_i \ln\left(\frac{z-1}{e}\right)\right]\left(\frac{\varphi_a}{r_a}\ln\varphi_a + \frac{\varphi_c}{r_c}\ln\varphi_c\right)\right\}^{-1}\end{aligned} \tag{12}$$

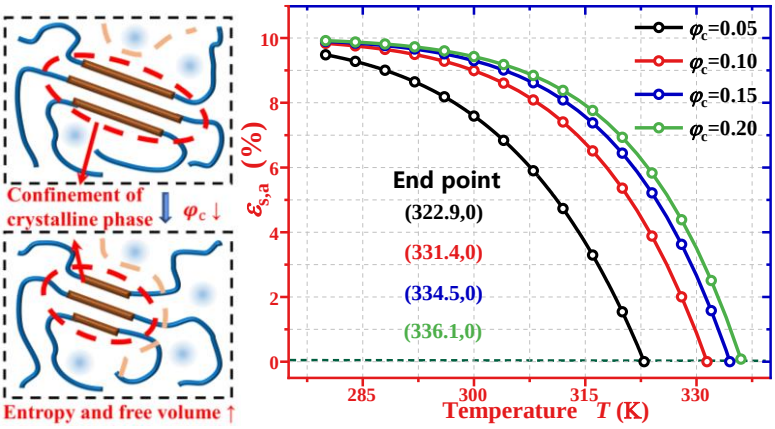

Fig. 2. The constitutive relationship of the stored strain of amorphous phase ($\varepsilon_{s,a}$) as a function of temperature at different volume fractions of crystalline phases of 5%, 10%, 15% and 20%.

To identify the dynamic confinement of crystalline phase on the glass transition behavior of amorphous phase, the stored strains of the amorphous phase ($\varepsilon_{s,a}$) as a function of temperature were calculated using equation (12), and the results are plotted in Fig. 2. The parameters used in equation (12) are A_0=5, m=3.6, F_a=8000 J/mol, $s^*\cdot\Delta\mu$=3020 J/mol [Macedo *et al.*, 1965], R_c/r_0=0.9 [Wang *et al.*, 2021], γ=γ_i=0.75 [Wang *et al.*, 2021], z=4 [Treloar, 2005] and $\varepsilon_{pre,a}$=10% [Luo *et al.*, 2010]. It is revealed that the phase transitions of

amorphous phase are completed at 322.9 K, 331.4 K, 334.5 K and 336.1 K, with the volume fraction of crystalline phase (φ_c) increased from 5%, 10%, 15% to 20%, respectively. These analytical results reveal that the crystalline phase has a significant confinement effect on the transition behavior of the amorphous phase. A lower volume fraction of crystalline phase is able to achieve a lower T_g of the amorphous phase, due to that the glass transition is able to complete at a lower temperature.

To further verify the dynamic confinement of crystalline phase on the amorphous phase in the semi-crystalline SMP, equation (12) was applied to predict the shape recovery behavior of DGEBA-NGDE/PCL (DGEBA: diglycidyl ether of bisphenol-A; NGDE: neopentyl glycol diglycidyl ether; PCL: poly(ε-caprolactone)) semi-crystalline SMP [Luo *et al.*, 2010], where the DGEBA-NGDE and PCL function as amorphous and crystalline phases, respectively. Values of parameters used in equation (12) during calculation are listed in Table 1, where $s^*{\cdot}\Delta\mu$=5950J/mol [Macedo *et al.*, 1965], $r_a/r_c=1.1\times10^5$, R_c/r_0=0.9, $\gamma=\gamma_i$=0.75 [Wang *et al.*, 2021] and z=4 [Treloar, 2005].

Table 1. Values of parameters used in equation (12) for DGEBA-NGDE/PCL semi-crystalline SMP. D and N are used to represent the DGEBA and NGDE, respectively.

	A_0	m	F_a (KJ/mol)	$\alpha_r(K^{-1})$	$\alpha_g T_0$	$\varepsilon_{pre,s}$ (%)	$\varepsilon_{pre,c}$ (%)	$\varepsilon_{pre,a}$ (%)
D20N80/PCL	1.008	1.005	10.015	0.03259	9.622	29.81	24.73	5.08
D30N70/PCL	1.150	1.038	9.757	0.03255	9.838	30.30	24.18	6.12
D40N60/PCL	1.200	1.042	9.618	0.03180	9.952	30.19	22.60	7.59

As shown in Fig. 3(a), the analytical results obtained using the proposed model are in good agreements with the experimental data reported in Ref. [Luo *et al.*, 2010]. The T_g value of DGEBA-NGDE/PCL SMP is gradually increased from 302.3 K, 304.6 K to 314.5K with the volume fraction of DGEBA increased from 20%, 30% to 40%, where the stored strain is released from 30% to 25%. This is mainly contributed to the effect of DGEBA, whose T_g value is higher than that of NGDE in an amorphous phase, resulting in the increase of T_g of DGEBA-NGDE/PCL SMP with an increase in the volume fraction of DGEBA. At the same time, the effect of crystalline phase on glass transition of two amorphous DGEBA and NGDE phases is not changed, due to that the volume fraction of PCL is kept constant. Then, the T_g of DGEBA-NGDE/PCL SMP is enhanced owing to the increase in the volume fraction of DGEBA. Fig. 3(b) shows the calculated divergences between the analytical and experimental results of the DGEBA-NGDE/PCL SMPs, e.g., the correlation index (R^2), which are 98.37%, 99.62% and 99.61% for D20N80/PCL, D30N70/PCL and D40N60/PCL SMPs, respectively. Clearly, good agreements between the analytical and experimental results [Luo *et al.*, 2010] are achieved, where the error ratio is limited to 1.5%.

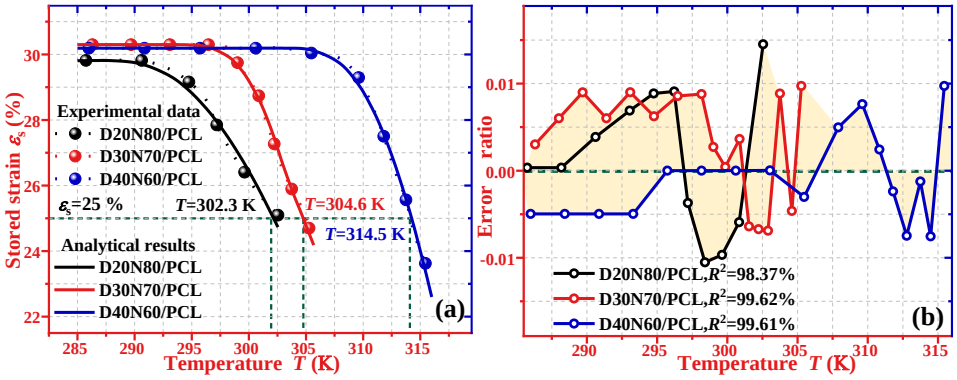

Fig. 3. Analytical results and experimental data [Luo *et al.*, 2010] of stored strain as a function of temperature for the DGEBA-NGDE/PCL semi-crystalline SMPs, heating rate at about 3 K/min. (a) The stored strain-temperature curves. (b) Divergences of the analytical and experimental results.

2.2. *Melting transition of crystalline phase*

Based on Avrami theory [Avrami, 1939] the frozen volume theory [Liu *et al.*, 2006], the volume evolution function of the crystalline phase ($\phi_c(T,t)$) has the following relationship with the temperature (T) and time (t),

$$\phi_c(T,t)=\frac{\varepsilon_{s,c}}{\varepsilon_{pre,c}}=\exp\left\{-K_{max}\int_0^t \exp\left[\frac{-4}{D^2}\ln\left(2\left(T-T_m\right)^2\right)\right]dt\right\} \tag{13}$$

where $\varepsilon_{s,c}$ and $\varepsilon_{pre,c}$ are the stored strain and pre-stored strain, respectively, K_{max} is the kinetic parameter of the melting transition and D is a given constant [Jeziorny *et al.*, 1978].

Based on the Gibbs-Thomson model [Hohne, 2002], the T_m is determined by the dimension of the single crystal (l_c), which can be written as,

$$T_m=T_m^0\left(1-\frac{2\gamma_e}{\Delta H_f l_c}\right) \tag{14}$$

where T_m^0 is the melting temperature of infinite crystal, γ_e is the free energy of interfacial melt-crystal phase and ΔH_f is the fusion heat [Hohne, 2002].

As discussed in Ref. [Mandelkern, 2004], the relationship between T_m and crystallizing temperature (T_c) can be obtained as,

$$2T_m=T_m^0+T_c \tag{15}$$

By substituting equation (14) into (15), T_c can be obtained as,

$$T_c=T_m^0\left(1-\frac{4\gamma_e}{\Delta H_f l_c}\right) \tag{16}$$

In combination of equations (13) and (14), the volume evolution function of crystalline phase ($\phi_c(T,t)$) can be obtained as follows,

$$\phi_c(T,t)=\frac{\varepsilon_{s,c}}{\varepsilon_{pre,c}}=\exp\left\{-K_{max}\int_0^t \exp\left[\frac{-4}{D^2}\ln\left(2\left(T-T_m^0+\frac{2\gamma_e T_m^0}{\Delta H_f l_c}\right)^2\right)\right]dt\right\} \quad (17)$$

Based on the equation (17), we can calculate the stored strain of crystalline phase ($\varepsilon_{s,c}$) as a function of temperature for the semi-crystalline SMP, and the obtained analytical results are shown in Fig. 4. The values of the parameters used in the equation (17) are listed in Table 2, where K_{max}=0.05, D=18.447 K and $\varepsilon_{pre,c}$=25% [Luo *et al.*, 2010]. In the calculation, the heating temperature (T) is replaced by the expression: $T=\dot{T}t+T_0$, where $\dot{T}$ is heating rate, T_0 the initial temperature and t is the time for heating. As presented in Fig. 4(a), the analytical results show that the stored strain of crystalline phase ($\varepsilon_{s,c}$) is gradually decreased with an increase in the temperature. The temperatures of melting transition are 305.9 K, 301.9 K, 297.9 K and 293.9 K, with an increase in unit of crystals γ_e from 10.0 mN/m, 12.5 mN/m, 15.0 mN/m to 17.5 mN/m at a given value of l_c=8 nm. On the other hand, the melting transition are completed at 295.2 K, 301.9 K, 305.9 K and 310.9 K, with an increase in l_c from 6 nm, 8 nm, 10 nm to 12 nm at a given value of γ_e=12.5 mN/m, as shown in Fig. 4(b). It is revealed that the free energy of interfacial melt-crystal phase (γ_e) and dimension unit of the single crystal (l_c) play essential roles to determine the melting transition behavior of crystalline phase.

Table 2. Values of parameters used in equation (17).

l_c=8 nm	T_m^0(K)	γ_e =12.5 mN/m	T_m^0(K)
γ_e=10.0 mN/m	304.0	l_c=6 nm	293.3
γ_e=12.5 mN/m	300.0	l_c=8 nm	300.0
γ_e =15.0 mN/m	296.0	l_c=10 nm	304.0
γ_e =17.5 mN/m	292.0	l_c=12 nm	306.7

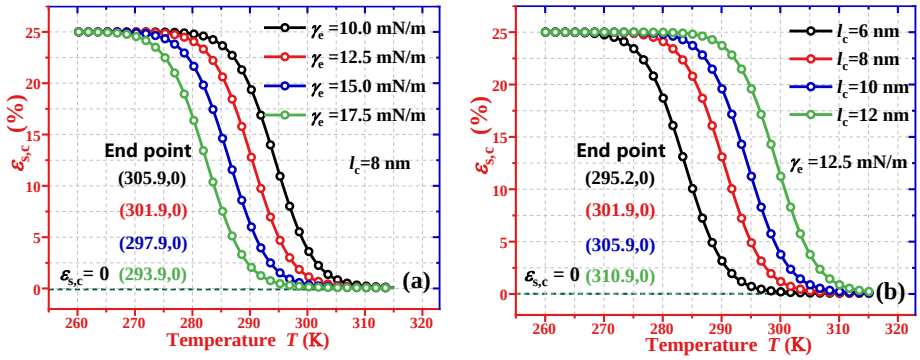

Fig. 4. Analytical results of the stored strain of crystalline phase ($\varepsilon_{s,c}$) as a function of temperature, heating rate at about 5 K/min. (a) Analytical curve of stored strain ($\varepsilon_{s,c}$) as a function of temperature at γ_e=10.0 mN/m, 12.5 mN/m, 15.0 mN/m and 17.5 mN/m. (b)

Analytical curve of stored strain ($\varepsilon_{s,c}$) as a function of temperature at l_c=6 nm, 8 nm, 10 nm and 12 nm.

Experimental data of PCL semi-crystalline SMPs (reported in Ref. [Scalet *et al.*, 2018]) were then used to further verify the results obtained using the newly proposed model. The values of the parameters in the calculation using equation (17) are summarized in Table 3, where γ_e=10.0 mN/m and l_c=10 nm. Fig. 5(a) illustrates the dynamic confinements mechanisms of amorphous and crystalline phases in the semi-crystalline SMP undergoing melting and crystallization transitions, respectively. The difference in melting and crystallization of crystalline phase is originated from their interfacial confinements with the amorphous phase, i.e., melt-crystal and amorphous-crystal confinements in melting and crystallization transitions, respectively. As plotted in Fig. 5(b), the volume fraction of crystalline phase (φ_c) of PCL-2 SMP is decreased from 23.08% to 0.99% with an increase in temperature from 233.4 K to 299.6 K. These analytical and experimental results reveal that the T_m and T_c of PCL-2 SMP are 299.6 K and 259.2 K, respectively.

Table 3. Values of parameters used in equation (17) for PCL semi-crystalline SMP.

		K_{max}	T_m^0(K)	ΔH_f (MJ/m^3)	D(K)
PCL-2	Heating	0.05	299.56	5.99	18.447
	Cooling	0.01	259.20	30.30	
PCL-3	Heating	0.145	318.34	5.99	
	Cooling	0.145	297.59	30.30	

On the other hand, the volume fraction of crystalline phase (φ_c) of PCL-3 SMP is decreased from 37.12% to 0.83% with an increase in temperature from 263.6 K to 311.9 K, where the T_m and T_c of PCL-3 SMP are 311.9 K and 284.1 K, respectively, as shown in Fig. 5(c). These analytical and experimental results reveal that both the Tm and T_c of PCL SMPs have been significantly increased with an increase in the volume fraction of crystalline phase (φ_c). However, the difference in T_m and T_c is decreased from 40.4 K (for PCL-2) to 37.8 K (for PCL-3) with an increase in the φ_c. The reason accounts for it is the interfacial confinement effect of the amorphous phase is decreased with the increase of the φ_c, resulting into the interfacial confinements between two phases therefore decreased.

Finally, the divergences between the analytical and experimental results are calculated based on the correlation index (R^2), of which the values are 99.46% and 99.38% for PCL-2 SMP in the heating and cooling processes, respectively, as well as 98.66% and 99.38% for PCL-3 SMP in the heating and cooling processes, respectively, as shown in Fig. 5(d). Clearly, the obtained analytical results using our newly proposed model fit well with the experimental ones of PCL SMPs [Scalet *et al.*, 2018].

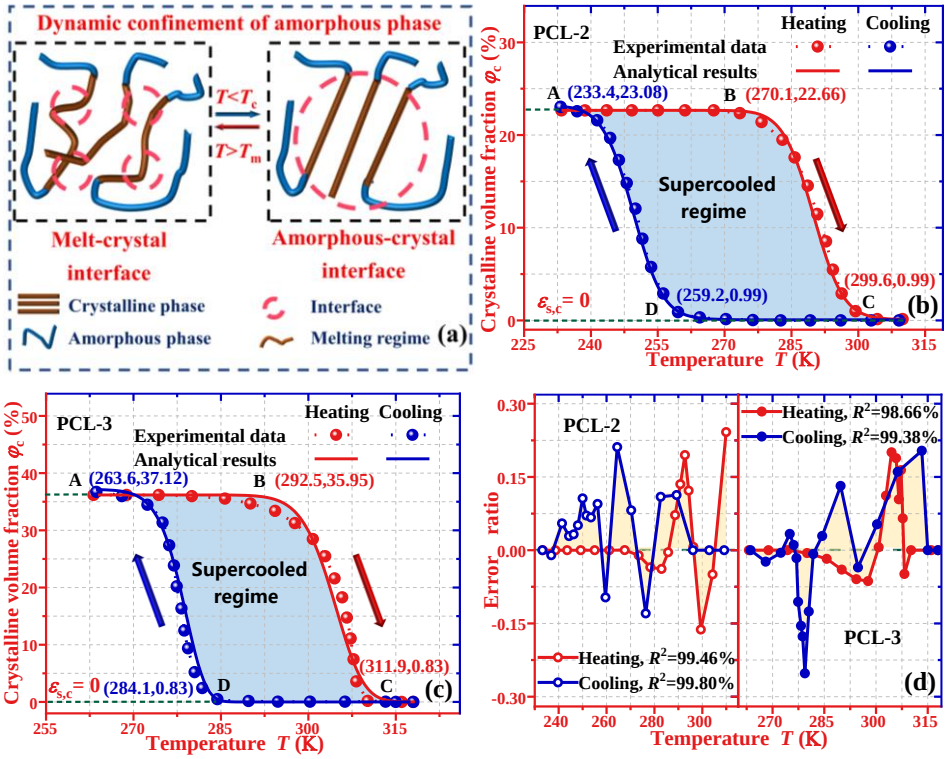

Fig. 5. Analytical and experimental results [Scalet *et al.*, 2018] of volume fraction (φ_c) as a function of the temperature for PCL SMPs, heating or cooling rate at about 2 K/min. (a) Schematic illustrations of dynamic confinements of melt-crystal-amorphous interfaces. (b) For the supercooled regime in PCL-2 SMP. (c) For the supercooled regime in PCL-3 SMP. (d) Divergences of the analytical and experimental results.

During the melting transition, the stored strain of semi-crystalline SMP (ε_s) is composed of both the crystalline phase ($\varepsilon_{s,c}$) and pre-stretch (ε_{s0}), i.e., $\varepsilon_s=\varepsilon_{s,c}+\varepsilon_{s0}$, as the glass transition had been completed before melting transition. Therefore, the stored strain of melting transition in semi-crystalline SMP (ε_s) can be obtained as,

$$\varepsilon_s=\varepsilon_{s,c}+\varepsilon_{s0}=\varepsilon_{pre,c}\exp\left\{-K_{max}\int_0^t\exp\left[\frac{-4}{D^2}\ln\left(2\left(T-T_m^0+\frac{2\gamma_e T_m^0}{\Delta H_f l_c}\right)^2\right)\right]dt\right\}+\varepsilon_{s0} \quad (18)$$

To understand the effect of melting transition on the stored strain in semi-crystalline SMP, equation (18) was applied to predict the stored strain results of a semi-crystalline SMP: PEVA-BPO (PEVA: poly (ethylene-co-vinyl acetate); BPO: benzoyl peroxide) [Hui *et al.*, 2020]. The obtained theoretical results are shown in Fig. 6. Values of parameters used in equation (18) during calculation are listed in Table 4, where γ_e=12.0 mN/m, l_c=12 nm and ΔH_f=5.99 MJ/m^3. The PEVA with 4 wt% BPO, 6 wt% BPO and 8 wt% BPO are named as PEVA-B4, PEVA-B6 and PEVA-B8, where the volume fractions of crystalline

phase (φ_c) are 14.13%, 13.94% and 13.38%, respectively [Hui *et al.*, 2020]. Fig. 6(a) shows that the proposed model can well predict the experimental results. By increasing the volume fraction of BPO from 4 wt%, 6 wt% to 8 wt%, the T_m is then decreased from 353 K, 350 K to 348 K, which is mainly contributed to the decrease in volume fraction of PEVA crystalline phase. With a lower volume fraction of PEVA, less thermal energy is needed for the melting transition in semi-crystalline SMP. Therefore, the melting transition is triggered at a lower temperature, resulting into a decreased value of T_m. Furthermore, the divergences between the analytical and experimental results are calculated based on the correlation index (R^2), and the obtained results are 95.75%, 98.78% and 98.39% for PEVA-B4, PEVA-B6 and PEVA-B8, respectively, as shown in Fig. 6(b). These results indicate that good agreements between the analytical and experimental results have been achieved, where the error ratio is limited to ±2%.

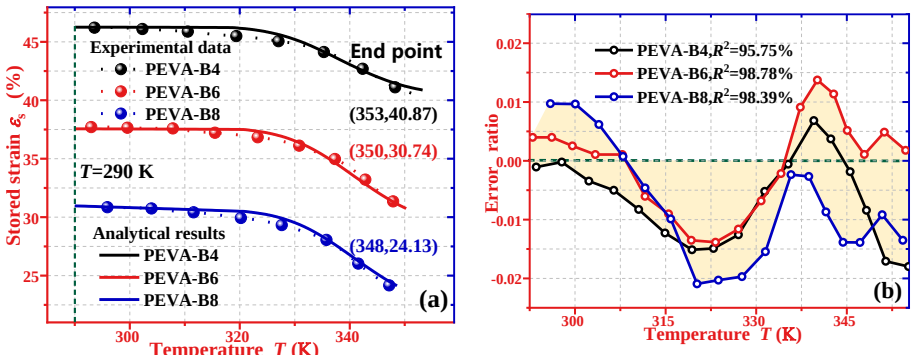

Fig. 6. Analytical results of equation (18) and experimental data [Hui *et al.*, 2020] of stored strain as a function of the temperature for the PEVA-BPO SMPs, heating rate at about 3 K/min. (a) For the stored strain-temperature curves. (b) Divergences of the analytical and experimental results.

Table 4. Values of parameters used in equation (18) for PEVA-BPO SMPs.

	φ_c(%)	K_{max}	T_m^0(K)	D(K)	ε_s(%)	ε_{s0}(%)	$\varepsilon_{pre,c}$ (%)
PEVA-B4	14.13	0.006	326.17	24.822	46.26	40.87	5.39
PEVA-B6	13.94	0.005	329.17		37.56	30.74	6.82
PEVA-B8	13.38	0.004	331.17		31.76	24.13	7.63

3. Multiple SMEs in semi-crystalline SMP

The Maxwell principle can be used to describe the storage modulus ($E(T)$) of semi-crystalline SMP as follows [Arruda *et al.*, 1993; Treloar *et al.*, 2005],

$$\frac{1}{E(T)} = \frac{1-\varphi_c}{E_a(T)} + \frac{\varphi_c}{E_c(T)} \tag{19}$$

where $E_a(T)$ and $E_c(T)$ are the storage moduli of the amorphous and crystalline phases in a semi-crystalline SMP, respectively.

The storage modulus of amorphous phase can be expressed as [Yang *et al.*, 2016],

$$\begin{aligned} E_a(T) &= E_{a0} \cdot \frac{\varepsilon_{s,a}}{\varepsilon_{pre,a}} \\ &= E_{a0} - E_{a0} \cdot A_0 T^m \exp\left(-\frac{F_a}{RT}\right) \\ &\cdot \exp\left\{ \begin{array}{l} \left[\frac{R^2 T}{s^* \Delta\mu} \cdot \frac{\varphi_c}{r_c}\left[\ln\varphi_c + \tanh\left(\frac{R_c}{r_0}-1\right)\frac{4\varphi_c - 3\varphi_c^2}{\varphi_a^2}\right] - \frac{\varphi_a}{\gamma}\cdot\left[\exp\left(\alpha_r T - \alpha_g T_0\right) - 1\right]\right]^{-1} \\ + \frac{R^2 T}{s^* \Delta\mu} \cdot \left[1 - \gamma_i \ln\left(\frac{z-1}{e}\right)\right]\left(\frac{\varphi_a}{r_a}\ln\varphi_a + \frac{\varphi_c}{r_c}\ln\varphi_c\right) \end{array} \right\} \end{aligned} \tag{20}$$

where E_{a0} is the initial storage modulus of the amorphous phase.

As reported in Ref. [Ge *et al.*, 2013], the storage modulus of the crystalline phase can be written as follows,

$$\begin{aligned} E_c(T) &= E_{c0} \cdot \frac{\varepsilon_{s,c}}{\varepsilon_{pre,c}} \\ &= E_{c0} \exp\left\{-K_{max}\int_0^t \exp\left[\frac{-4}{D^2}\ln\left(2\left(T - T_m\right)^2\right)\right]dt\right\} \end{aligned} \tag{21}$$

where E_{c0} is the initial storage modulus of crystalline phase.

By substituting equations (20) and (21) into equation (19), the storage modulus of semi-crystalline SMP can be obtained as,

$$\frac{1}{E(T)} = \frac{1-\varphi_c}{E_{a0}(T)\cdot\frac{\varepsilon_{s,a}}{\varepsilon_{pre,a}}} + \frac{\varphi_c}{E_{c0}\cdot\frac{\varepsilon_{s,c}}{\varepsilon_{pre,c}}} \tag{22}$$

Using equation (22), we have calculated the storage modulus of PEVA-BPO semi-crystalline SMP, and then the analytical results are compared with those experimental data reported in Ref. [Hui *et al.*, 2020], as shown in Fig. 7. The input values in equations (20), (21) and (22) are φ_c=22.85% [Hui *et al.*, 2020], E_{a0}=3 GPa, A_0=9.6×10^{-3}, m=1, F_a=2026.80 J/mol, φ_a/γ=0.8, α_r=0.02831 K^{-1}, $\alpha_g T_0$=4.2, E_{a0}=8520.95 MPa [Hui *et al.*, 2020], K_{max}=0.02, T_m^0=370 K [Hui *et al.*, 2020], D=138.28 K, $s^*\cdot\Delta\mu$=1359.6 kJ/mol [Macedo *et al.*, 1965], r_a/r_c=1.1×10^5, R_c/r_0=0.9, γ_i=0.75 [Wang *et al.*, 2021] and z=4 [Treloar, 2005]. Fig. 7(a) plots the analytical results of the storage modulus as a function of temperature for the PEVA-BPO SMP. The experimental data reported in Ref. [Hui *et al.*, 2020] and the analytical results were plotted for comparisons. The analytical results obtained from the proposed model are in well agreement with the experimental ones. The dynamic storage modulus is gradually decreased from 2526.7 MPa to 91.8 MPa due to the glass transition of PEVA component from 195 K to 261 K; and then it is further decreased from 91.8 MPa to 0.4 MPa due to the melting transition of BPO component range from 261 K to 362 K. Moreover, the divergences between the analytical and experimental results are calculated

based on the correlation index (R^2), of which the values are 97.25% and 82.67%, respectively, as shown in Fig. 7(b). These results indicate that the proposed model is suitable to predict the experimental results by taking the dynamic confinements of amorphous and crystalline phases into consideration during modelling for semi-crystalline SMP.

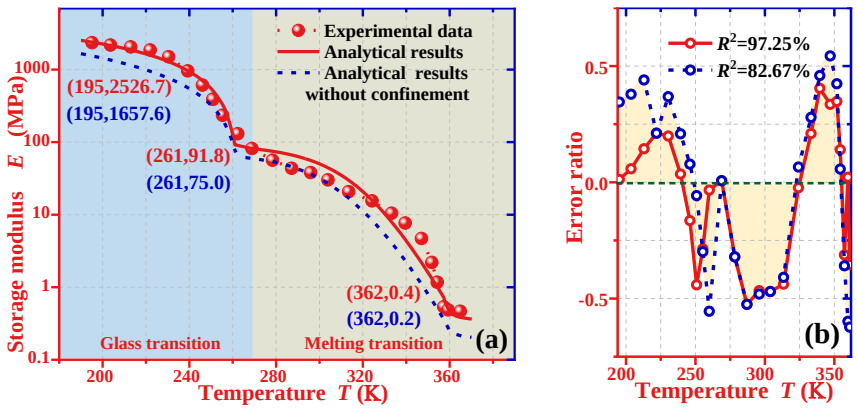

Fig. 7. (a) Comparisons among analytical results using equation (22), using the no-confined model, and experimental data [Hui *et al.*, 2020] of the storage modulus as a function of temperature, heating rate at about 3 K/min. (b) Divergences of the analytical and experimental results.

On the other hand, the stored strain (ε_s) is composed of both of the amorphous phase ($\varepsilon_{s,a}$) and crystalline phase ($\varepsilon_{s,c}$) as well as the initially stored strain (ε_{s0}), i.e., $\varepsilon_s=\varepsilon_{s,a}+\varepsilon_{s,c}+\varepsilon_{s0}$, when a semi- crystalline SMP undergoes both glass and melting transitions. According to the Maxwell principle [Arruda *et al.*, 1993; Treloar *et al.*, 2005], the stored strain of semi-crystalline SMP (ε_s) can be obtained based on the equations (10) and (17) as follows,

$$\begin{cases} \varepsilon_s=\sum_{i=1}^{n_a}\varepsilon_{s,a}(i)+\sum_{j=1}^{n_c}\varepsilon_{s,c}(j)=\sum_{i=1}^{n_a}\varepsilon_{pre,a,i}\exp\left(-\dfrac{t-t_{a,i}}{\tau_{0,a,i}}\right)+\sum_{j=1}^{n_c}\varepsilon_{pre,c,j}\phi_{c,j}(T,t)+\varepsilon_{s0} \\ \tau_{0,a,i}=\tau_{0,i}\exp\left(\dfrac{F_{a,i}}{RT}\right) \\ \cdot\exp\left\{\begin{array}{l}\dfrac{-R^2T}{s^*\Delta\mu}\cdot\dfrac{\varphi_c}{r_c}\left[\ln\varphi_c+\tanh\left(\dfrac{R_c}{r_0}-1\right)\dfrac{4\varphi_c-3\varphi_c^2}{\varphi_a^2}\right]+\dfrac{\varphi_a}{\gamma}\cdot\left[\exp\left(\alpha_r T-\alpha_g T_0\right)-1\right] \\ +\dfrac{R^2T}{s^*\Delta\mu}\cdot\left[\gamma_i\ln\left(\dfrac{z-1}{e}\right)-1\right]\left(\dfrac{\varphi_a}{r_a}\ln\varphi_a+\dfrac{\varphi_c}{r_c}\ln\varphi_c\right)\end{array}\right\}^{-1} \\ \phi_{c,j}(T,t)=\dfrac{\varepsilon_{s,c,j}}{\varepsilon_{pre,c,j}}=\exp\left\{-K_{max}\int_{t_{c,j}}^{t}\exp\left[\dfrac{-4}{D^2}\ln\left(2\left(T-T_m^0+\dfrac{2\gamma_e T_m^0}{\Delta H_f l_c}\right)^2\right)\right]dt\right\} \end{cases} \tag{23}$$

where n_a and n_c are the numbers of the glass and melting transitions in the semi-crystalline SMP, respectively. i represents the ith glass transition of the amorphous phase, j represents the jth melting transition of the crystalline phase. $t_{a,i}$ and $t_{c,j}$ are the starting times of the ith

glass transition and *j*th melting transition, respectively. $\tau_{0,a,i}$ and $\tau_{0,c,j}$ are the relaxation times of the *i*th glass transition of amorphous transition and *j*th melting transition, respectively.

The experimental results for two types of semi-crystalline SMPs, e.g., PLLA-PEB (PLLA: poly(L-lactic acid); PEB: poly(ethylene-cobutylene)) and PLLA-PEB-PDLA (PDLA: poly(D-lactic acid))[Zhou *et al.*, 2018] were used to verify their multiple SMEs using our newly proposed model of equation (23).The data for the parameters in the calculation using equation (23) are listed in Table 5, where $\tau_{0,a}$=2.241 min, K_{max}=0.6 and D=18.447 K. The obtained results are shown in Fig. 8.

The analytical results and experimental data [Zhou *et al.*, 2018] show that a dual-SME has been achieved in the PLLA-PEB SMP, which undergoes sequential glass and melting transitions of PLLA phase, as shown Fig. 8(a). During the two-step shape recovery behavior, the stored strain is initially decreased from 82.34% to 28.87% in the temperature range from 293.5 K to 328.5 K owing to the glass transition of PLLA. Then it is decreased from 28.87% to 3.57% in the temperature range from 328.5 K to 363.5 K owing to the melting transition of PLLA. The PLLA-PEB SMP takes 16.1 minutes to complete the first-step shape recovery, and then it takes 22 minutes to complete the second-step shape recovery. Meanwhile, the divergences between the analytical and experimental results of PLLA-PEB SMP are calculated based on the correlation index (R^2), of which the values are 98.51% and 94.29%, respectively, as shown in Fig. 8(b).

Furthermore, equation (23) is used to predict the triple-SME in PLLA-PEB-PDLA SMP. As shown Fig. 8(c), both the analytical results and experimental data [Zhou *et al.*, 2018] show that a triple-SME has been achieved in the PLLA-PEB-PDLA SMP, which undergoes sequential glass and melting transitions of PLLA phase, and then the melting transition of PDLA phase. A three-step shape recovery behavior has been revealed, where the stored strain is initially decreased from 72.55% to 41.25% in the temperature range from 293.5 K to 333.5K owing to the glass transition of PLLA. And then it decreased from 41.25% to 24.64% in the temperature range from 333.5K to 363.5K owing to the melting transition of PLLA. Finally, it decreased from 24.64% to 4.60% in the temperature range from 363.5K to 403.5K owing to the melting transition of PDLA. The PLLA-PEB-PDLA SMP takes 15.4 minutes to complete the first-step shape recovery, and then it takes 16.8 minutes to complete the second-step shape recovery. Finally, it takes 17.5 minutes to complete the third-step shape recovery. The divergences between the analytical and experimental results of PLLA-PEB-PDLA SMP are calculated based on the correlation index (R^2), which are 99.64% and 95.66%, as shown in Fig. 8(d).

Table 5. Values of parameters used in equation (23) for PLLA-PEB and PLLA-PEB-PDLA SMPs.

	$\varepsilon_{pre,a}$(%)	ε_{pre}(%)	ε_0(%)	t_a(min)	t_c(min)	T_m (K)
PLLA-PEB	65.16	28.50	2.95	77.48	93.52	350.60
PLLA-PEB-PDLA	34.66	18.06	4.52	134.76	150.07	351.44
		18.60			166.84	395.8

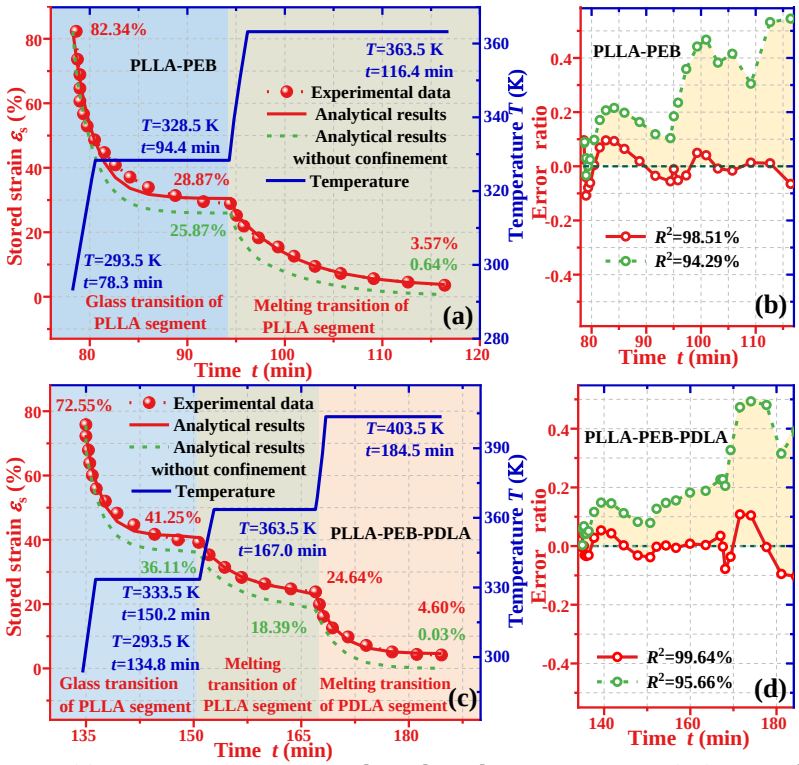

Fig. 8. (a) Comparisons among analytical results using equation (23), using the no-confined model, and experimental data [Zhou *et al.*, 2018] of the storage modulus as a function of temperature for PLLA-PEB SMP undergoing two-step shape recovery, heating rate at about 10 K/min. (b) Divergences of the analytical and experimental results, where the correlation index are R^2=98.51% and R^2=94.29%. (c) Comparisons among analytical results using equation (23), using the no-confined model, and experimental data [Zhou *et al.*, 2018] of the storage modulus as a function of temperature for PLLA-PEB-PDLA SMP undergoing three-step shape recovery, heating rate at about 10 K/min. (d) Divergences of the analytical and experimental results, where the correlation index are R^2=99.64% and R^2=95.66%.

4. Conclusion

In this study, a dynamic confinement model was firstly developed to describe the multiple SMEs in semi-crystalline SMP. A confinement entropy model is initially formulated to investigate the glass transition of amorphous phase, where the dynamic confinement signature is proposed using the free volume and its connection to crystalline phase in semi-crystalline SMP. Moreover, a modified Avrami model is developed to characterize the melting transition of the crystalline phase. Furthermore, the sequentially dynamic relaxations have been investigated and discussed for the semi-crystalline SMPs, and the predictions of their dual-SME and triple-SME have been achieved. The interfacial

confinements of melt-crystal and amorphous-crystal have been identified as the driving force for the supercooled regime in semi-crystalline SMPs. Finally, the effectiveness of our newly proposed model has been verified by the experimental data of semi-crystalline SMPs, including DGEBA-NGDE/PCL, PCL, PEVA-BPO, PLLA-PEB and PLLA-PEB-PDLA reported in the literature. This study aims on a new mechanism of the dynamic confinement and also critical insights into the cooperative principle of coexisting amorphous and crystalline phases in the semi-crystalline SMP towards multiple SMEs.

Acknowledgments

This work was financially supported by the National Natural Science Foundation of China (NSFC) under Grant No. 11725208 and 12172107, and International Exchange Grant (IEC/NSFC/201078) through Royal Society and NFSC.

References

Avrami, M. [1939] "Kinetics of phase change. I: general theory," *Journal of Chemical Physics* **7**(12), 1103–1112.

Adams, P.A., Sheppard, J.G., Ridler, G.M., Ridler, P.F. [1978] "New three-parameter empirical extension of the Arrhenius equation suitable for the precise evaluation of pseudo-thermodynamic activation parameters in chemical kinetics," *Journal of the Chemical Society, Faraday Transactions 1: Physical Chemistry in Condensed Phases*. **74**(0), 1500–1506.

Arruda, E.M., Boyce, M.C. [1993] "Evolution of plastic anisotropy in amorphous polymers during finite straining," *International Journal of Plasticity* **9**(6), 697–720.

Bellin, I., Kelch, S., Langer, R., Lendlein, A. [2006] "Polymeric triple shape materials," *Proceeding of The National Academy of Sciences of The United States of America* **103**(48), 18043−18047.

Cohen, M.H., Turnbull, D. [1959] "Molecular transport in liquids and glasses," *Journal of Chemical Physics* **31**, 1164–1169.

Cho, J.W., Kim, J.W., Jung, Y.C., Goo, N.S. [2005] "Electroactive shape-memory polyurethane composites incorporating carbon nanotubes," *Macromolecular Rapid Communications*. **26**(5), 412–416.

Doolittle, A.K. [1951] "Studies in newtonian flow: II. The dependence of the viscosity of liquids on free-space," *Journal of Applied Physiology* **22**, 1471.

Dickie, R.A. [1973] "Heterogeneous Polymer-Polymer Composites. I. Theory of Viscoelastic Properties and Equivalent Mechanical Models," *Journal of Applied Polymer Science* **17**, 45–63.

Fang, Y., Ni, Y.L., Leo, S.Y., Taylor, C., Basile, V., Jiang, P. [2015] "Reconfigurable photonic crystals enabled by pressure-responsive shape-memory polymers," *Nature Communications* **6,** 7146.

Fang, C.Q., Leng, J.S., Sun, H.Y., Gu, J. P. [2018] "A multi-branch thermoviscoelastic model based on fractional derivatives for free recovery behaviors of shape memory polymers," *Mechanics of Materials* **120**, 34–42.

Gibbs, J.H., Adam, G. [1965] "On the temperature dependence of cooperative relaxation properties in glass-forming liquids," *Journal of Chemical Physics* **43**, 139–146.

Ginzburg, V. V. [2005] "Influence of Nanoparticles on Miscibility of Polymer Blends: A Simple Theory," *Macromolecules* **38**(6), 2362–2367.

Ge, Q., Luo, X.F., Iversen, C.B., Mather, P.T., Dunn, M.L., Qi, H.J. [2013] "Mechanisms of triple-shape polymeric composites due to dual thermal transitions," *Soft Matter* **9**(7), 2212–2223.

Hohne, G.W.H. [2002] "Another approach to the Gibbs-Thomson equation and the melting point of polymers and oligomers," *Polymer* **43**(17), 4689 – 98.

Hamonic, F., Prevosto, D., Dargent, E., Saiter. A. [2014] "Contribution of chain alignment and crystallization in the evolution of cooperativity in drawn polymers," *Polymer* **55**(12), 2882–2889.

Hui, J., Xia, H., Chen, H.R., Qiu, Y.P., Fu, Y.Q., Ni, Q.Q. [2020] "Two-way reversible shape memory polymer: Synthesis and characterization of benzoyl peroxide-crosslinked poly(ethylene-co-vinyl acetate)," *Materials Letters* **258**, 126762.

Huang, R., Zheng, S.J., Liu, Z.S., Ng, T.Y. [2020] "Recent advances of the constitutive models of smart materials-hydrogels and shape memory polymers," *International Journal of Applied Mechanics* **12**(2), 2050014.

Hu, J.Y., Toh, W., Ng, T.Y., Jiang, N., Zeng, L.S., Du, J.K., Liu, Z.S. [2021] "Inhomogeneous large deformation study on magneto-thermal sensitive hydrogels," *International Journal of Applied Mechanics* **13**(5), 2150053.

Jäckle, J. [1986] "Models of the glass transition," *Reports on Progress in Physics* **49**(2), 171–231.

Jeziorny, A. [1978] "Parameters characterizing kinetics of nonisothermal crystallization of poly(ethyleneterephthalate) determined by DSC," *Polymer* **19**(10), 1142–4.

Ji, S.B., Fan, F.Q., Sun, C.X., Yu, Y., Xu, H.P. [2017] "Visible light-induced plasticity of shape memory polymers," *ACS Applied Materials & Interfaces* **9**(38), 3169–3175.

Liu, Y.P., Gall, K., Dunn, M.L., Greenberg, A.R., Diani, J. [2006] "Thermomechanics of shape memory polymers: uniaxial experiments and constitutive modeling," *International Journal of Plasticity* **22**(2), 279–313.

Lee, K.J., Lee, D.K., Kim, Y.W., Choe, W.S., Kim, J.H. [2010] "Theoretical consideration on the glass transition behavior of polymer nanocomposites," *Journal of Polymer Science Part B-Polymer Physics* **45**(16), 2232–2238.

Luo, X.F., Mather, P.T. [2010] "Triple-Shape Polymeric Composites (TSPCs)," *Advanced Functional Materials* **20**(16), 2649–2656.

Lu, H.B., Liang, F., Gou, J.H. [2011] "Nanopaper enabled shape-memory nanocomposite with vertically aligned nickel nanostrand: controlled synthesis and electrical actuation," *Soft Matter* **56**(7), 7416–7423.

Macedo, P.B., Litovitz, T.A. [1965] "On the relative roles of free volume and activation energy in the viscosity of liquids," *Journal of Chemical Physics* **42**, 245 – 256.

Mandelkern, L. 2004 Crystallization of Polymers Cambridge: Cambridge University Press.

Meng, H., Li, G.Q. [2013] "A review of stimuli-responsive shape memory polymer composites," *Polymer* **54**(9), 2199–2221.

Ortega, J.M., Hartman, J., Rodriguez, J.N., Maitland, D.J. [2013] "Virtual treatment of basilar aneurysms using shape memory polymer foam," *Annual Review of Biomedical Engineering* **41**(4), 725–43.

Qin, H.H., Mather, P. T. [2009] "Combined one-way and two-way shape memory in a glass-forming nematic network," *Macromolecules* **42**(1), 273−280.

Schweizer, K.S., Saltzman, E.J. [2004] "Theory of dynamic barriers, activated hopping, and the glass transition in polymer melts," *Journal of Chemical Physics* **121**(4), 1984–2000.

Santo, L., Quadrini, F., Squeo, E.A., Dolce, F., Mascetti, G., Bertolotto, D., Villadei, W., Ganga, P.L., Zolesi, V. [2012] "Behavior of shape memory epoxy foams in microgravity: experimental results of STS-134 mission," *Microgravity Science and Technology* **24**(4), 287–296.

Scalet, G., Pandini, S., Messori, M., Toselli, M., Auricchio, F. [2018] "A one-dimensional phenomenological model for the two-way shape-memory effect in semi-crystalline networks," *Polymer* **158**, 130–148.

Treloar, L.R.G. 2005 The Physics of Rubber Elasticity New York: Oxford University.

Vili, Y.Y.F.C. [2007] "Investigating smart textiles based on shape memory materials," *Textile Research Journal* **77**(5), 290–300.

Wang, S., Brigham, J.C. [2012] "A computational framework for the optimal design of morphing processes in locally activated smart material structures," *Smart Materials and Structures* **21**(10), 105016.

Wang, X.D., Jian, W., Lu, H.B., Lau, D., Fu, Y.Q. [2021] "Selective entanglement coupling of nanoparticles in polymer nanocomposite with high shape recovery stress," *Composites Science and Technology* **207**, 108728.

Xie, T. [2010] "Tunable polymer multi-shape memory effect," *Nature* **464**(7286), 267−270.

Yang, B., Huang, W.M., Li, C., Lee, C.M., Li, L. [2004] "On the effects of moisture in a polyurethane shape memory polymer," *Smart Materials and Structures* **3**, 191–195.

Yang, Q.X., Li, G.Q. [2016] "Temperature and rate dependent thermomechanical modeling of shape memory polymers with physics based phase evolution law," *International Journal of Plasticity* **80**, 168–186.

Zhou, J., Cao, H.Q., Chang, R.X., Shan, G.R., Bao, Y.Z., Pan, P.J. [2018] "Stereocomplexed and Homochiral Polyurethane Elastomers with Tunable Crystallizability and Multishape Memory Effects," *ACS Macro Letters* **7**(2), 233-238.

Zhang, Y.F., Zhang, N.B., Hingorani, H., Ding, N.Y., Wang, D., Yuan, C., Zhang, B., Gu, G.Y., Ge, Q. [2019] "Fast-response, stiffness-tunable soft actuator by hybrid multimaterial 3D printing," *Advanced Functional Materials* **29**(15), 1806698.

Zheng, S.J., Liu, Z.S. [2021] "The machine learning embedded method of parameters determination in the constitutive models and potential applications for hydrogels," *International Journal of Applied Mechanics* **13**(1), 2150001.